Robust phase retrieval using group-delay-dispersion-scanned second harmonic generation demonstrated in a femtosecond fiber chirped-pulse amplification system

Yujun Feng, Johan Nilsson and Jonathan H. V. Price

***Abstract*— We propose and demonstrate a phase retrieval method using a novel variant of the dispersion scan ('d-scan') technique via both simulations and experimental measurements on a femtosecond fiber laser. The method combines a map of group-delay-dispersion-scanned (d-scan) second-harmonic generation (SHG) spectra together with the fundamental spectrum as inputs. In order to ensure the technique is robust when pulse-to-pulse fluctuations are present, we use only the wavelengths of the resulting SHG peaks, and avoid the areas with low signal in the borders of the data trace. Simulations confirmed the phase-retrieval is accurate even with high levels of laser fluctuation. The trade-off is that pulses which have abruptly changing or highly modulated phase profiles are not retrievable. The d-scan uses the compressor gratings intrinsic to the fiber chirped-pulse amplification (CPA) systems so the method is low cost. For experimental verification, we used a 470 fs ytterbium-fiber CPA system, so the method is applicable to measurements on fiber based fs laser systems which generally have an order of magnitude less bandwidth than the Ti:sapphire lasers used to test earlier variants of the d-scan approach.**

***Index Terms*—) Fiber optics amplifiers and oscillators, Ultrafast measurements, Ultrafast nonlinear optics**

I. Introduction

THE characterization of ultrashort laser pulses has been an active research field for many years and several measurement approaches are now available. For pulses that are close to transform-limited, the inclusion of spectral data enables full characterization, e.g. via PICASO [1], in cases where a second-harmonic generation (SHG) autocorrelation (AC) [1] would leave ambiguities about the pulse profile. In the more general case, the widely known SHG frequency resolved optical gating (FROG) technique [2, 3], which uses spectrally resolved autocorrelation (or cross-correlation) data is a good solution developed more than a decade ago. FROG has since led to variants such as GRENOUILLE, which is available as a commercial instrument [4]. However, FROG is based on an interferometric scheme, which demands precise alignment. Methods related to the technique of spectral phase interferometry for direct electric-field reconstruction (SPIDER) [5] use an analytic formula to solve the problem of phase retrieval from the data but the data-recording setup is usually more complex than that used for FROG.

To avoid the need for the precise interferometric alignment required for FROG and SPIDER, an alternative set of methods that do not require division of the pulse has emerged based on scanning an externally applied phase. One of the first such approaches, termed MIIPS (multiphoton intrapulse interference phase scan), uses an optical arrangement with a spatial light modulator (SLM) to apply computer controlled spectral-phase changes [6, 7].

To enable non-interferometric measurements when a spectral phase controller is not available, d-scan methods were developed using the SHG spectra obtained when changing the applied GDD with prisms. Typically the fundamental spectrum has been used as a self-consistency check [8-11]. However, these are complex algorithms, and inclusion of data in the wings of the SHG spectra which are most sensitive to noise may mean the methods become less robust when characterizing lasers with significant output fluctuations. Indeed, when simpler algorithms have been tested, they were found to fail in cases where noise is present [12].

Motivated by the attractions of non-interferometric methods such as MIIPS and d-scans (i.e. simplicity; intuitive data-interpretation) and the need for low-cost and robust characterization approaches, we developed a new phase retrieval method which is easy to implement and robust in the presence of pulse-to-pulse fluctuations. To this end, we developed a new hybrid d-scan approach with simple algorithm to enable rapid uptake by non-specialist users.

Manuscript received xx xx 2018; revised xx xx, 2018; accepted xx xx, 2018. Date of publication xx xx, 2018; date of current version xx xx, 2018. This work was supported in part by the Engineering and Physical Sciences Research Council UK (EPSRC) (EP/M014029/1, EP/P012248/1); Air Force Office of Scientific Research (AFOSR) (FA9550-14-1-0382). . (Corresponding author: Jonathan H. V. Price. Email: jhvp@soton.ac.uk)

Yujun Feng Johan Nilsson and Jonathan H. V. Price are with the Optoelectronics Research Centre, University of Southampton, Southampton SO17 1BJ, UK

All data supporting this study are openly available from the University of Southampton repository at https://doi.org/10.5258/SOTON/D0414.

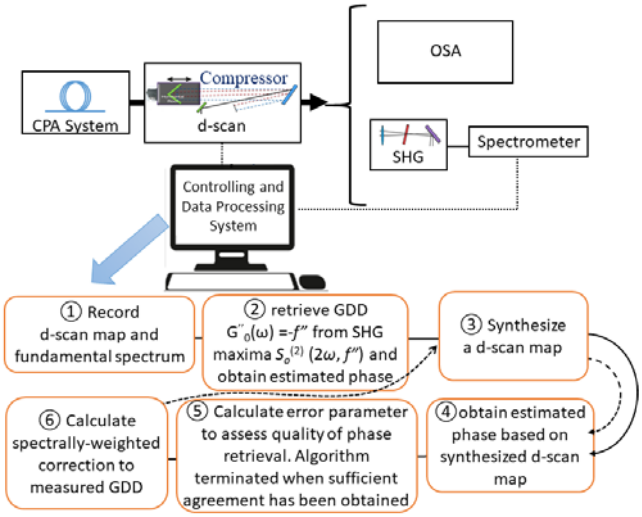

Fig. 1. (Color online.) Schematic of the phase retrieval process. (GDD: group delay dispersion.). See text for details of the algorithm.

We were interested in supporting our fiber laser development which involved relatively long pulse durations of the order of 300 fs (i.e. bandwidths approximately an order of magnitude less than that previously reported in d-scan retrieval papers using sub-30 fs pulses from Ti:sapphire lasers [8, 10, 13]). Our long pulse durations require a much larger GDD scan range, e.g. $\pm 2 \times 10^6$ fs^2 was used in our simulations and experiments compared to values of the order of $\pm 5 \times 10^3$ fs^2 with a 30 fs Ti:sapphire laser. Our low-cost setup lacks the degrees of freedom provided by the SLM used in a MIIPS measurement, which would apply corrections to iteratively flatten the phase via repeated d-scans. There, the pulse quality is iteratively improved as phase corrections are applied. We use only a single d-scan and add the fundamental spectrum to improve the estimate of the pulse phase through computational iterations.

We demonstrate the usefulness of the resulting method by showing that it correctly retrieves the phase of a wide range of pulse shapes with durations in the 100-500 fs range, with the exception of pulses having stepped phase profiles or phase profiles with high frequency modulations. (These modulated pulses are known to be challenging with d-scan methods [14].) We did not extensively focus on the requirement for mathematically proven properties but checked that the phase measurements remain correct via both simulations and experiments when the typical pulse-to-pulse fluctuations studied by others [15, 16] were present in the data.

The structure of the paper is as follows: Section 2 describes the theory and outlines the algorithm. Section 3 shows the results of numerical simulations using data without pulse-to-pulse fluctuations. Section 4 shows simulation results when pulse-to-pulse fluctuations are introduced. Section 5 shows experimental results from an Yb fiber CPA system. Finally, Section 6 provides a discussion and summary.

II. THEORY

A schematic of the measurements required and the steps of the retrieval algorithm are shown in Fig. 1. The input data are the fundamental spectrum and the SHG spectra *vs*. applied GDD, $\varphi_a'' = \partial^2\varphi_a/\partial\omega^2$, i.e., the d-scan map. The applied GDD is determined by the compressor setting. As shown in step 1 the GDD is scanned to create the SHG d-scan map and the fundamental spectrum is also measured.

The algorithm is then based on the equation for the SHG spectrum shown below [14]:

$$S^{(2)}(2\omega) \propto \left|\int |E(\omega+\Omega)||E(\omega-\Omega)| \times exp\{i[\varphi(\omega+\Omega)+\varphi(\omega-\Omega)]\}\, d\Omega\right|^2. \quad (1)$$

Here ω and $2\,\omega$ are optical frequencies, $S^{(2)}(2\omega)$ represents the SHG power spectrum, $E(\omega)$ represents the fundamental amplitude spectrum, $\varphi(\omega)$ is the spectral phase and Ω is the integration variable. Typically only ranges of Ω in which the phase argument $\varphi(\omega+\Omega)+\varphi(\omega-\Omega)$ is constant or slowly varying, can make significant contributions to this integral. The main assumptions in Eq. (1) are that the SHG process is instantaneous and spectrally uniform, both of which are reasonable for the longer-than 100-fs pulses typical for fiber lasers. In many practical cases, the phase can be expanded as a Taylor series around ω, as shown in Equation (2),

$$\varphi(\omega+\Omega)+\varphi(\omega-\Omega) = 2\varphi(\omega)+\varphi''(\omega)\Omega^2 + \sum_{n=2}^{\infty}\frac{2}{(2n)!}\varphi^{(2n)}(\omega)\Omega^{2n}. \quad (2)$$

This function is symmetric in Ω. If the phase variations are sufficiently smooth, then the dominant contribution to the integrand in Eq. (1) is expected to occur when $\varphi''(\omega) = 0$. If an additional GDD of $\varphi_a''(\omega)$ is applied, then the SHG maxima are expected to occur for values of ω where the second derivative of the phase of the pulse, $\varphi''(\omega)$, exactly cancels that of the applied GDD so that $\varphi_{total}''(\omega) = 0$.

Therefore, like MIIPS, our approach starts by applying a known wavelength-dependent GDD function and assumes that the majority of the SHG at a given frequency arises where the applied GDD matches that of the pulse. In MIIPS, the applied GDD is re-scanned iteratively to further optimize the GDD estimate because Eq. (1) shows that the SHG at frequency $2\,\omega$ also contains a contribution from pairs of frequencies offset by $\pm\,\Delta\omega$ from ω. It is possible that these contributions result in a slowly-varying phase of the integrand in Eq. (1) over an extended range of frequencies, and thus become significant, for an applied GDD function which differs from that for which $\varphi_{total}''(\omega) = 0$. To take this global influence into account, the MIIPS scan is run repeatedly with refined GDD functions to improve the flatness of the phase of the final pulse until it finds the GDD function f'' (which includes higher order dispersion) that makes the pulse essentially transform limited and thus cancels the original phase of the pulse, typically after approximately five iterations.

Table I lists definitions for the symbols. The subscripts denote the stage of the algorithm progress: '*o*' – the original measured d-scan data, used to provide the first estimate of the GDD of the pulse: '*i*' – the estimate of a parameter on the i^{th} iteration; and '*r*' - the retrieved value after algorithm convergence has been completed and *'a'* is the applied GDD.

Next, with reference to the steps in Fig. 1, we describe the algorithm in detail. Step 1 records $S_o^{(2)}(2\omega, f'')$ and $S(\omega)$).

In step 2, the algorithm estimates the GDD of the pulse by assuming that at each wavelength, the pulse GDD is equal in amplitude and opposite in sign to the applied GDD for which the SHG reaches its maximum. An estimate of the spectral phase (phase *vs*. frequency) is then obtained by integrating twice. Thus, for each ω, attain $\varphi_o''(\omega) = G_o''(\omega)$ as the positions of the maxima of $S_o^{(2)}(2\omega, f'')$ and integrate twice to get $\varphi_o(\omega)$.

In step 3, this phase estimate is used together with the measured fundamental spectrum to synthesize a d-scan map, which will be similar to, but slightly different from, the measured d-scan map. i.e., an updated d-scan map, $S_i^{(2)}(2\omega, f'')$ is created through simulations based on S (ω) and most recently found phase $\varphi_i(\omega)$ (starting from $\varphi_o(\omega)$).

Step 4 is similar to step 2, but uses the synthesized d-scan map instead of the measured one to re-estimate the GDD positions of the SHG peaks to obtain a revised $G_i''(\omega)$.

In step 5, we use the difference between the synthesized and measured SHG maxima from step 4 to assess the retrieval quality and hence the degree of success of the process. If this is not adequate, then the phase profile is updated and steps 3 – 6 are repeated until the retrieval process is deemed to have succeeded, or alternatively failed. After typically five iterations there is close agreement between the synthesized and measured d-scan map. The error metric is given by $Err_{Gi} = \int |G_{ei}''(\omega)| d\omega$ as shown in Eq. (3) and explained below.

In step 6, the positions of the synthesized and measured SHG maxima are both used to update the estimate of the pulse GDD, $\varphi''(\omega)$, from the previous step using a spectrally weighted fraction of the difference between the GDD-values of the synthesized (G_i'') and measured (G_o'') SHG maxima using $G_{ei}''(\omega) = S_M(\omega)(G_i''(\omega - G_o''(\omega))$. The spectral weighting is to make the convergence more consistent. The GDD estimate is updated to $\varphi_{i+1}''(\omega) = \varphi_i''(\omega) + G_{ei}''(\omega)$ and this is integrated twice to obtain the new spectral phase $\varphi_{i+1}(\omega)$. We then take $\varphi_r(\omega) = \varphi_{i+1}(\omega)$ as final retrieved phase.

(In step 6 we also tried to adjust the GDD estimate by the whole and half of the difference, but the convergence was inconsistent.)

TABLE I
DEFINITION OF SYMBOLS IN THE PAPER

Symbol	Definition
$\boldsymbol{\omega}$	Angular frequency
$\boldsymbol{S(\omega)}$	Fundamental power spectrum
$\boldsymbol{S_M(\omega)}$	Fundamental power spectrum scaled so that max $S_M(\omega) = 1$
$\boldsymbol{S_{o,i,r}^{(2)}(2\omega)}$	SHG power spectrum (original/ith iteration/retrieved)
$\boldsymbol{\varphi_{o,i,r,a}(\omega)}$	Phase profile in frequency domain (original/ith iteration/retrieved/applied)
$\boldsymbol{\varphi''_{o,i,r,a}(\omega)}$	Estimated GDD (group delay dispersion) (original/ith iteration/retrieved/applied)
$\boldsymbol{f''}$	applied GDD for d-scan
$\boldsymbol{S_{o,i,r}^{(2)}(2\omega, f_j'')}$	d-scan SHG spectrum map (original/ith iteration/retrieved)
$\boldsymbol{G''_{o,i,r}(\omega)}$	GDD *vs*. frequency as determined as the values of the applied GDD for which the SHG $\mathbf{S_{o,i,r}^{(2)}(2\omega, f_j'')}$ reaches its maximum for each ω. (original/ith iteration/retrieved)
$\boldsymbol{Err_\varphi}$	Integrated spectrally weighted phase error Eq. (5)
$\boldsymbol{G_e''(\omega)}$	Local spectrally weighted GDD error Eq. (3)
$\boldsymbol{Err_G}$	Integrated spectrally weighted GDD error $\int \mathbf{G_e''(\omega)} d\omega$ Eq. (3)
$\boldsymbol{Err_m}$	Integrated global d-scan map error Eq. (4)

As a refinement to ensure convergence when the simulated or experimental data includes noise, a numerical smoothing step was applied to $G_i''(\omega)$ by using the 'Loess' function [17] within Matlab. This applies a local regression using weighted linear least squares and a 2nd degree polynomial model. The weighting of the Loess function was chosen to be the nearest ~10% of the total spectrum.

Three error metrics have been used to quantify the retrieval quality. The first two show the difference between the retrieved and measured d-scan data. The first calculates the local error of the SHG peak position, as that is the quantity used by the algorithm to find the phase and to check the convergence. It shows the spectrally weighted difference between SHG maxima positions G'' on the measured and synthesized d-scan map:

$$Err_G = \int |G_e''(\omega)| d\omega = \int S_M(\omega) |G_r''(\omega) - G_o''(\omega)| d\omega. \quad (3)$$

$G_r''(\omega)$ is the line through the SHG maxima on the synthesized d-scan map, $G_o''(\omega)$ is the line of SHG maxima from the measured d-scan map. The weighting from the fundamental spectrum, $S_M(\omega)$, is scaled so that the maximum of $S_M(\omega)$ equals unity, i.e. $S_M(\omega) = S(\omega)$ /max ($S(\omega)$), and $G_e''(\omega) = S_M(\omega)(G_i''(\omega) - G_o''(\omega))$.

The second error metric captures the global error across the entire d-scan, including points at the edges, to check that the local convergence leads to global convergence across the d-scan. It uses the root-mean-square (rms) difference between the measured and synthesized data for all the data points in the d-scan map. The calculation is similar to that used to quantify a FROG retrieval error and could also be used to compare our method with other d-scan methods.

$$\mathrm{Err_m} = \sqrt{\frac{1}{\mathrm{N_i N_j}} \sum_{\mathrm{i,j}} \left(\mathrm{S_o^{(2)}}(2\omega_\mathrm{i}, \mathrm{f_j''}) - \mu \mathrm{S_r^{(2)}}(2\omega_\mathrm{i}, \mathrm{f_j''}) \right)^2}. \quad (4)$$

Here $S_r^{(2)}(2\omega_i, f_j'')$ and $S_o^{(2)}(2\omega_i, f_j'')$ are the normalized retrieved and measured SHG spectral power densities at frequency $2\omega_i$ and GDD f_j'' (which is scanned across the GDD range so f_j'' is the scan variable), and μ is a factor that minimizes the error [10].

For the simulations the applied phase profile of the pulse is known, enabling a third error metric, Err_φ, to be used as a direct measure of the phase retrieval accuracy:

$$\mathrm{Err_\varphi} = \int \frac{S_M(\omega)}{\int \mathrm{S_M}(\omega) d\omega} |\varphi_\mathrm{r}(\omega) - \varphi_\mathrm{o}(\omega)| \mathrm{d}\omega. \quad (5)$$

Here $\varphi_r(\omega)$ and $\varphi_o(\omega)$ are the retrieved and original spectral phase profiles.

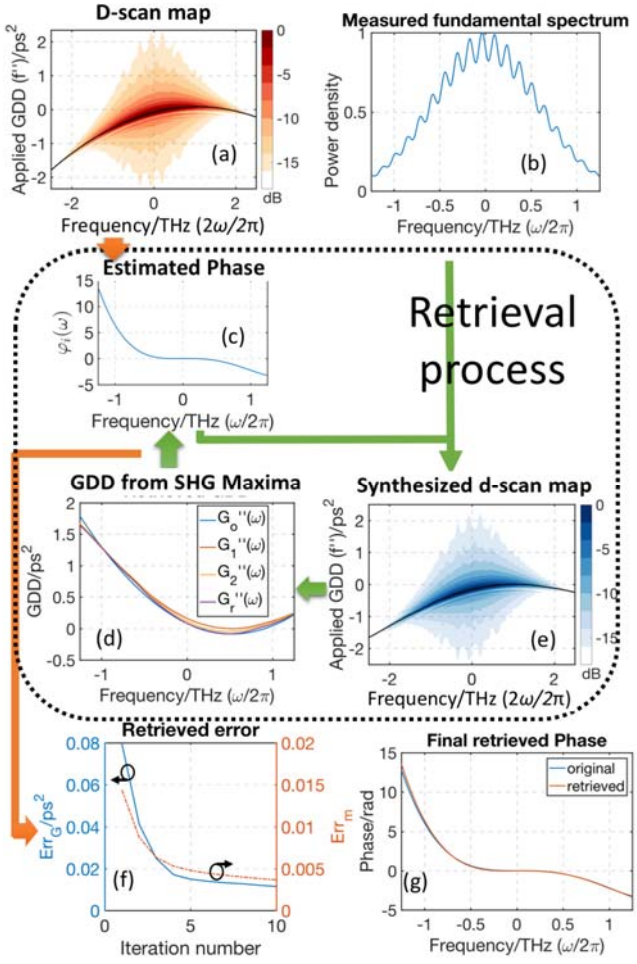

Fig. 2. (Color online.) Illustrative data at different steps of the phase retrieval. (a) Stitched-colormap showing SHG spectra calculated using Eq. (1) for different applied GDD (d-scan map); (b) fundamental spectrum; (c) estimated phase $\varphi(\omega)$ obtained by second integral of estimated GDD $\varphi''(\omega)$; (d) Estimated retrieved GDD in successive iterations, $G_i''(\omega)$, (e) Synthesized d-scan using retrieved phase and the fundamental spectrum; (f) spectrally weighted retrieved GDD error (Eq. 3) and global error (Eq. 4) illustrating typical evolution to a low plateau value *vs*. iteration number; (g) comparison of finally retrieved phase and the applied spectral phase.

Typical data are illustrated in Fig. 2. The simulations show a pulse with a modulated Gaussian spectrum. Fig. 2(a) shows the d-scan map $S_o^{(2)}(2\omega, f'')$. The frequencies shown in this and subsequent figures are the offset from the pulse's centroid frequency. The colormap has a logarithmic scale running from 0 dB in dark shades to –20 dB in white. The SHG maxima, $G_o''(\omega)$, are linked by the overlaid black line. The pulse spectrum is shown in Fig. 2(b). The iterative phase retrieval is illustrated by the arrows. The estimated phase $\varphi_i(\omega)$ is shown in Fig. 2(c). The GDD $G_i''(\omega)$ as the SHG maxima of the synthesized d-scan map at 1, 2 and 5 iterations is shown in Fig. 2(d). A synthesized d-scan $S_i^{(2)}(2\omega, f'')$ as obtained using the estimated phase and the fundamental spectrum is shown in Fig. 2(e). The line shown through the data at the SHG maxima, $G_i''(\omega)$, is compared with that in Fig. 2(a) so a correction can be calculated for the next iteration. The resulting Err_G and global error, Err_m, both rapidly decrease as the algorithm converges (Fig. 2(f)). The finally retrieved phase $\varphi_r(\omega)$ and actual phase of the simulated pulse are a close match as shown in Fig. 2(g).

The applied phase in this simulation has third and fourth order dispersion (TOD, FOD) of: TOD = -0.1 ps^3; FOD = 0.03 ps^4. The pulse bandwidth was 5 nm (full width at half maximum, (FWHM)) and the central wavelength was 1045 nm. This corresponds to a transform-limited Gaussian pulse with duration of 133 fs. We chose a GDD step of 0.094 ps^2, and a scan range of ±2.34 ps^2 which is the same as the experimental parameters (section V). The maximum applied GDD of ±2.34 ps^2 stretched the pulse to ~ 20 ps. In the algorithm, we set the total time range to be 100 ps (frequency step 0.01 THz) and so the 4096 grid-points provide a time-step of 24 fs. All simulations used 500 GDD steps and show results after five iterations.

III. EVALUATION OF APPROACH WITH NUMERICAL SIMULATIONS

Our simulations used both symmetric and asymmetric test-spectra and applied even, odd and random phase distortions as detailed in section III A. We investigated the algorithm performance where the dispersion scanning instrument (e.g., a grating compressor) has a calibration error (section III A). Self-phase-modulation (SPM) is a known distortion in fiber laser systems so the ability of the method to retrieve the phase-profile of a pulse with distortions from SPM is also shown (section III A). Special cases where the algorithm fails to perform are shown in section III B. The algorithm was next tested with double-pulses (section III C). Finally, to test retrieval in the presence of pulse-to-pulse fluctuations, we created averaged results for ensembles of pulses and then ran the retrieval algorithm on those datasets (section III D). All of the parameters and results are summarized in Table II.

A. Phase retrieval for pulses with symmetric and asymmetric spectral profiles

Tests were performed on pulses with a (symmetric) Gaussian power spectrum, and with an (asymmetric) right-triangle power spectrum. In all cases we aim for phase distortions that lead to the same temporal stretch ratio $r = \tau_{rms}/\tau_{TL}$, where τ_{rms} is the duration of the distorted pulse and τ_{TL} is the transform limited pulse duration (rms). We tested Taylor series dispersion profiles and a randomly generated phase profile which was created by first generating random phases in the range ± π/2 at each frequency grid-point, then applying a 0.2 THz low-pass filter to smooth the phase.

In Fig. 3, results for the right-triangle spectrum are shown. (Good results were also obtained for the Gaussian.) From the retrieval error values, Err_φ–shown inset, the best match was obtained with a 3rd order phase profile (Fig. 3(d)). In all cases the results converged to a stable phase profile in less than five iterations.

We chose to use a small GDD step size for all simulations as well as for the experiment to both maintain consistency and to ensure a single line of SHG maxima would be evident in the d-scan map. We tested whether a fine resolution for the applied GDD steps was required by simulating a Gaussian spectrum

with 4th order dispersion (0.03 ps^4) and with GDD step sizes ranging from 0.001 ps^2 to 0.01 ps^2. The results (not shown) indicated that as the GDD step increased, the retrieval error, Err_G, (Eq. 3), also increased from 0.0048 ps^2 to 0.012 ps^2. Furthermore, when we extended the investigation to pulses where the d-scan was more complex and had multiple secondary maxima, as was the case in the experimental section, we found that a coarse scan resulted in the algorithm making rapid switches between subsidiary maxima. Hence the coarse scan would, in general, need some form of pre-processing algorithm that analyzed the d-scan and the fundamental spectrum in order to fit the line through the global GDD *vs*. SHG maxima (i.e., *G*").

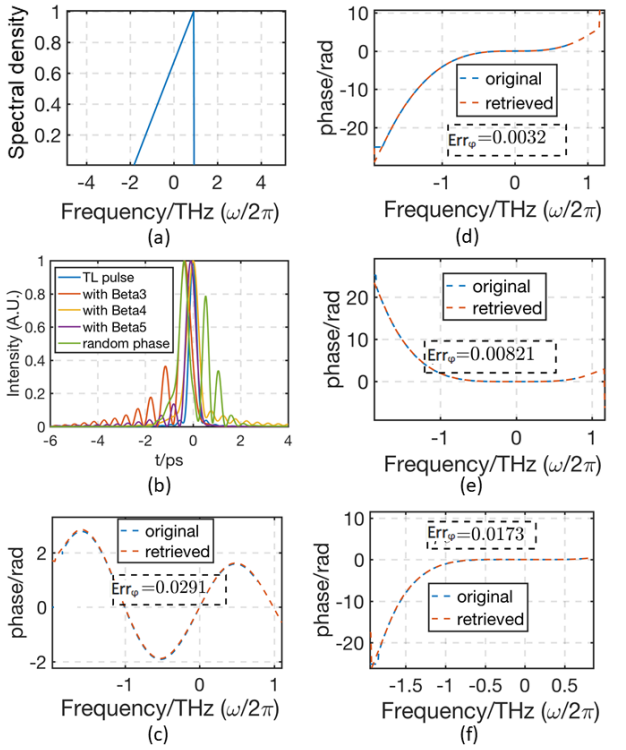

Fig. 3. (Color online.) Simulation results for pulse with an asymmetric right-triangular spectrum corresponding to a 133 fs transform-limited pulse with 3rd, 4th, 5th order dispersion or a randomly generated phase. (a) Pulse spectrum; (b) Time-domain profiles; (c)-(f) Test and retrieved phase profiles (retrieval error inset): (c) random phase; (d) 3rd order dispersion distortion; (e) 4th order dispersion; (f) 5th order dispersion.

We considered the effect of applied dispersion calibration errors potentially caused by uncertainty in the parameters of the compressor using the Gaussian test spectrum and the same phase profiles described above for the triangular pulse, but where the scanned GDD from the grating pair had an error of 5%, so that the GDD used in the retrieval algorithm was 5% larger than the true GDD. In the simulations without this calibration offset the retrieval errors Err_φ were 0.0282, 0.0575, 0.0569 and 0.0291 for the 3rd, 4th, 5th order and random phase profiles. With the calibration discrepancy, the retrieval error remained constant at 0.028 for the 3rd-order profile, and increased to 0.087, 0.0824 and 0.119 for the respective higher-order phase profiles. In principle the increase in retrieval error can, as with the case of FROG, be used not only to check the probable accuracy of the retrieved phase, but also can draw attention to the need for accurate calibration of the compressor GDD e.g. using a time-domain measurement such as the SHG autocorrelation to experimentally check the GDD calibration.

Finally in this section, we considered a pulse subject to self-phase-modulation (SPM) because in fiber lasers this nonlinearity is often a key limitation on pulse energy. We wished particularly to consider CPA systems so whereas for all other simulated pulses, the amplitude and phase profiles were parametrized directly, for this example only, we have performed additional calculations to obtain a realistic phase. We started with the above Gaussian spectrum, stretched the pulse to a duration of 1.0 ns by applying GDD, applied SPM with a peak nonlinear phase shift (B-integral) of 3 rad, then recompressed with the opposite GDD. (Note: Fourier grid based calculations would require an unwieldy 104 increase in grid size to directly calculate the SPM induced phase change on the stretched pulse so we used the simplified but still accurate phase calculation method developed in Ref. [18].) The retrieval results are shown in Fig. 4(a) and (b) and it is clear that across the majority of the pulse the phase retrieval is accurate.

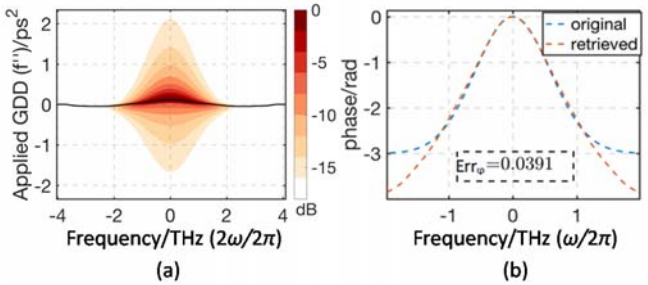

Fig. 4. (Color online.) Simulation results for Gaussian pulse with SPM applied (B-integral = 3 radians). (a) d-scan map.; and (b) simulated and retrieved phase profiles. (See text and Table 2 for details.).

B. *Limitations from special cases*

Cases that pose a special challenge for the algorithm are considered here. The auto-convolution in Eq. 1 shows that several frequencies offset to the side from the (2ω/2) frequency, ω, contribute via sum-frequency generation [10]. For simple phase profiles that can be represented using a few terms in a Taylor series, the phase of the sum-frequency generation will normally oscillate rapidly for frequencies away from the point where $\varphi''_{Total}(\omega) = 0$ in Eq. (1, 2) and therefore they do not contribute significantly to the SHG. Then the dominant contributor to the SHG at each point is from the directly related fundamental frequency as is assumed by the algorithm. However, when the phase varies in a less regular manner the SHG data can be distorted by the sum-frequency components. Pulses for which the spectral phase has abrupt changes or is highly modulated thus pose a challenge: e.g. rapid periodic phase modulations across a pulse could mean that if there are two or more equally offset frequencies that share the same GDD then they could contribute to a SHG maximum at an intermediate frequency where the GDD of the fundamental is in fact different. We therefore investigated this and some other special cases to check for errors.

The first results shown are for the standard Gaussian

spectrum with stepped phase change of π as shown in Fig. 5(a), (b). Accurate phase retrieval was not possible and the high error, Err_φ = 1.18, compared to 0.029 for the Gaussian spectrum with randomly generated but smoothly varying phase, confirms this. The performance is similar to MIIPS [19] ; but not as good as G-MIIPS [20] or FROG [3].

Next, a Gaussian spectrum with smoothly varying sinusoidal phase between 0 and π and one complete period within the spectral bandwidth (FWHM) was studied. The results in Fig. 5 (c), (d) show the retrieval is largely successful, with the phase being accurate at the center of the pulse and then showing small deviations at the edges. Here, Err_φ = 0.263 is, correspondingly, higher than the case of a Gaussian with random phase (Err_φ = 0.029) but below that of the stepped phase (Err_φ = 1.18). When the modulation frequency increased so there are four periods of a sinusoid with amplitude of π within the spectral half-bandwidth then the retrieval failed, as indicated in Fig. 5 (e), (f). In summary, expected challenges, e.g. a stepped-phase profile or a rapidly varying spectral phase profile were encountered, but the algorithm performed well provided the phase was slowly varying across the spectral bandwidth.

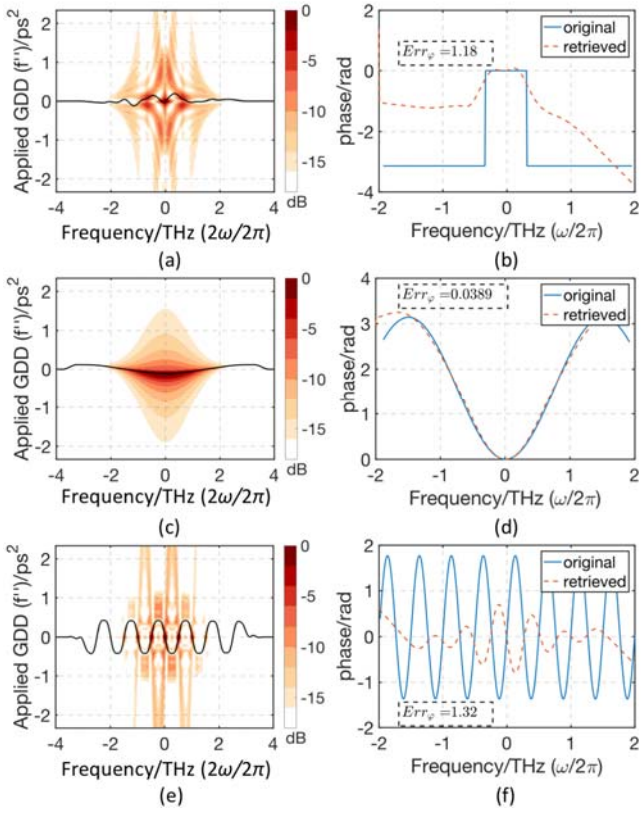

Fig. 5. (Color online.) Simulation results for special cases. The left column shows the d-scan maps. The right column shows the simulated and retrieved phase profiles. (a), (b) Gaussian with step change in phase profile; (c), (d) Gaussian with slowly varying sinusoidal phase profile; (e), (f) Gaussian with rapidly varying sinusoidal phase. (See text and Table 2 for details.)

C. Double pulse

Satellite pulses are commonly observed in practice and can be either created intentionally or appear via unwanted etalon effects or polarization splitting. A double pulse is normally considered more straightforward to detect with time domain measurements, such as a SHG autocorrelation, than with frequency based techniques such as d-scans, so it represents an important test.

1) Pre- or post-pulse replicas

The standard Gaussian pulse (Table II) was replicated and the replica's energy reduced to 4% of the main pulse. A temporal offset of ±5 ps was then applied to create a pre- or post-pulse, as is shown in Fig. 6 (a) (b). Fig. 6 (c) and (d) show the fundamental spectra with the expected modulations. The d-scans in Fig. 6 (e) and (f) are clearly different for pre- and post-pulses, enabling the temporal order to be determined. We found that the patterns remained qualitatively similar for other pulse separations and relative pulse phases, which suggests (but does not prove) that the approach is valid in general. In contrast, the widely adopted SHG autocorrelation technique would not clearly identify a pre-pulse or post-pulse, so this is valuable information, even though it requires consideration of the SHG spectral data across the d-scan map, not just the positions of the SHG maxima used by the algorithm.

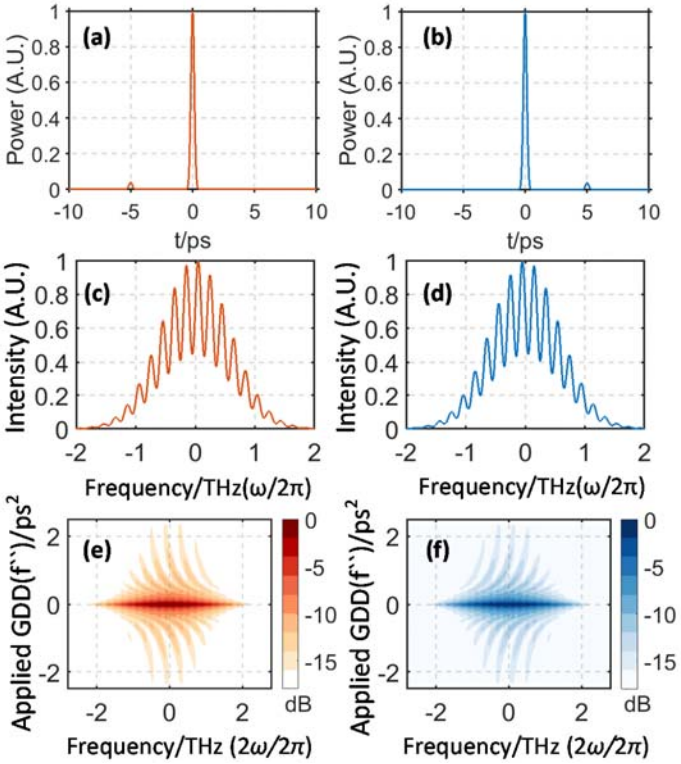

Fig. 6. (Color online.) Simulation results for a 4% replica pre-pulse (shown in (a,c,e)) and post-pulse (shown in (b,d,f)). Both the main pulse and the replica have identical, transform-limited, phase profiles. (a), (b) temporal profiles (c), (d) fundamental spectral profiles (same for pre- and post-pulse). (e), (f) d-scans. (The central line across the SHG data does have power density modulations similar to those in the fundamental spectra although the dB scale for the d-scan map in the lower row insets does not display this very clearly.)

2) Duplicate pulse having different phase profile from parent

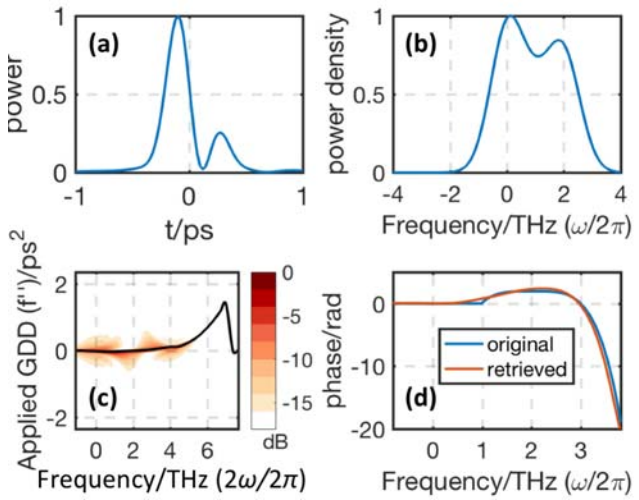

Fig. 7. (Color online.) Simulation results for complex double pulse profile (see text for details). (a) double pulse in time domain; (b) fundamental spectrum; (c) d-scan map; (d) actual (original) and retrieved phase results.

As a second test of double pulses, offset spectra and different phase profiles were considered. Two pulses were created with identical Gaussian spectra and the main pulse had a flat phase. Considering the spectral domain, the energy of the second pulse was 80% of that of the main pulse, and it had a frequency offset of 2 THz. At frequencies >1 THz from the center of the main pulse we applied a 4th order dispersion term centered on the secondary pulse. (The phase was made continuous at the join by offsetting the peak of the phase of the second pulse. See Table II.) Figure 7 (a, b) show the pulse is double-peaked in both the time and frequency domains. Figure 7(c) shows the d-scan data and Fig. 7(d) shows the applied and retrieved phase profile after five iterations. There is a discrepancy where the slope of the spectral-phase has a discontinuity, but otherwise the retrieval is reasonably accurate. The phase retrieval error, Err_{φ},was 0.5

D. Simulations with pulse-to-pulse fluctuations

This section assesses the effects of pulse-to-pulse fluctuations that will be present in any averaged experimental data. This is useful when the measurement equipment is unable to acquire required data from a single pulse and therefore has to average over several pulses. These effects are indeed perhaps the most significant uncertainty in a practical measurement. (For shot data, noise is normally not a large source of measurement uncertainty.) The pulse-to-pulse fluctuations considered are taken from ref [15], which reported a MIIPS based phase measurement. The authors described the range of potential fluctuations and how they may be inferred from different measurement systems [15, 16]. Firstly amplitude and secondly bandwidth fluctuations were chosen because they are commonly observed in Ti:sapphire lasers [15], and, thirdly, GDD fluctuations were considered because they have been reported when air-flows are present in laser compressors [16]. They indicated that their new 'fidelity' parameter provided an indicator of expected statistically-averaged laser performance in the context of image contrast in multiphoton microscopy so that given two otherwise similar laser sources, the one with higher fidelity would lead to brighter SHG images. As well as the practical need to be able to use our approach on lasers with fluctuations, our simulations were motivated by the possibility of using a d-scan to perform fidelity measurements in the future. As a first step, here we show that our algorithm correctly retrieves the average phase for the types of fluctuations considered in ref [15].

A spectrometer might record data over 10 ms, and would hence average over thousands of pulses during the data acquisition process if the laser has a repetition rate in the MHz range or just over tens of pulses for higher energy systems operating in the tens of kHz range. We created ensembles of 24 randomly generated pulses with amplitude or bandwidth fluctuations that had a Gaussian distribution and standard deviation of up to 20% of the mean value in 2% steps so there were a total of 11 simulations performed for each case.

The SHG spectra were calculated for every pulse in the ensemble and the SHG spectra were then averaged to create a target 'measurement' for our algorithm to fit. The fundamental spectrum used in the retrieval algorithm did not have pulse-to-pulse fluctuations applied. The fundamental spectrum would not show any variation when phase fluctuations are applied so it is expected to be more stable than the SHG. A further refinement could in principle consider noise applied to this data in addition to the SHG spectra. We considered the standard Gaussian and triangular pulses with 3rd, 4th, 5th and randomly generated GDD distortions (Table II). The results in Fig. 8. extend down to a standard deviation of zero, i.e. the fluctuation-free case.

The simulations with amplitude fluctuations used scaling ratio r_a that had a Gaussian distribution with unity mean and 0-20% standard deviation. It was applied by multiplying the spectrum with the scaling variable: $r_a \times S(\omega - \omega_0)$, where ω_0 is the centroid frequency ($\omega_0 = \int \omega\, S(\omega) d\omega / \int S(\omega) d\omega$

Simulations with spectral bandwidth fluctuations used a similar scaling variable r_b, applied using: $S((\omega - \omega_0)/r_b)/r_b$.

The third set of simulations applied GDD fluctuations corresponding to vibrations of the grating in the CPA compressor. A compressor mirror offset, ΔL, was considered by adding a term to the spectral phase using the formula $\varphi(\omega - \omega_0) + \beta_2 \Delta L (\omega - \omega_0)^2/2$, where $\beta_2 = 0.94$ ps²/rad/mm. The parameter ΔL had a mean of zero and standard deviation extending up to 0.1 mm in 0.01 mm steps such that there were a total of 11 separate simulations.

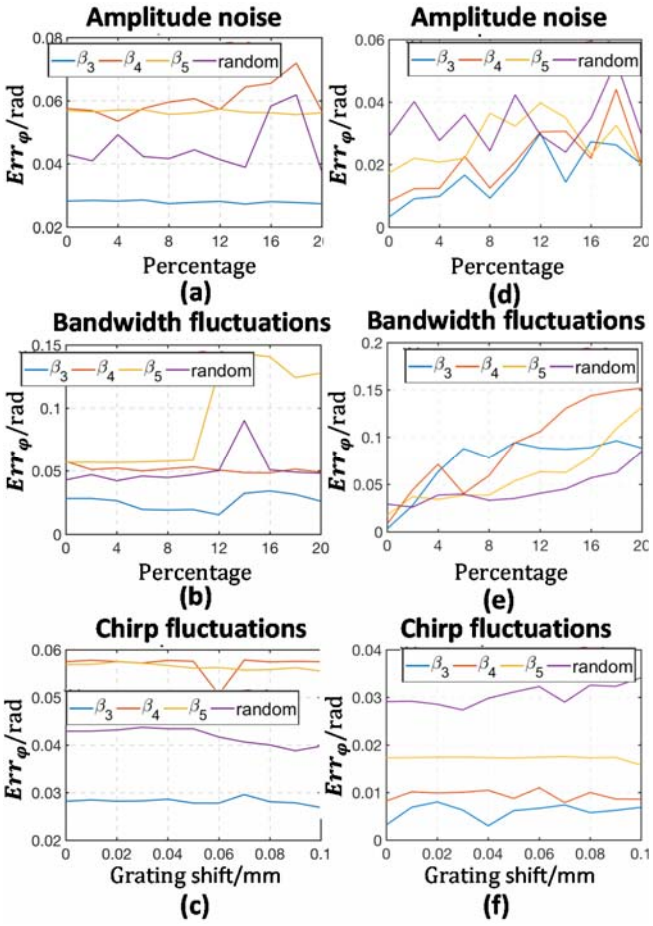

Fig. 8. (Color online.) The influence of pulse-to-pulse fluctuations on the phase retrieval accuracy. The test pulses are the same as in Section A, namely, a Gaussian (figures (a)-(c)) and right-triangular spectrum (figures (d)-(f)) with applied 3rd, 4th 5th order GDD and random GDD profiles. (See Table 2.) Each row shows the test results for a different type of pulse fluctuation.(See text for details.)

The results for the Gaussian pulse appear in the first column of Fig. 8. The results for the right-triangular shaped pulse in the second column of Fig. 8. Although there is no strong trend for in the retrieval error with increasing levels of fluctuations for either pulse shape for the case of amplitude fluctuations or GDD fluctuations, for the case of bandwidth fluctuations the triangular pulse showed a gradually increasing retrieval error. Even when applying the maximum error, we still were of the view when looking at the phase data (not shown) that the retrievals were largely successful. We are unsure why, the shape of the pulse is apparently important when considering bandwidth fluctuations. It may be due, at least in part, to the hard edged shape we selected. To enable comparison of the algorithm evaluation error with the results in the experimental section, we note that for the right-triangular spectrum with randomly generated GDD profile and bandwidth fluctuations of 15%, $Err_G = 5.59 \times 10^{-3}$ ps^2.

In general, the results in Fig. 8 demonstrated that the retrieval error did not steadily increase as the level of fluctuations increased. We concluded that since the method robustly retrieved the phase in the presence of high levels of the fluctuations considered that it should perform well in practice given the lower level of fluctuations that might be expected experimentally.

To test how the retrieval error changes with the number of pulses in the ensemble we considered the case of a triangular spectrum with randomly generated GDD and 15% bandwidth fluctuations. In the single shot-case (ensemble size of one pulse at each applied GDD value in the d-scan map), the data for sequential GDD points could include wide fluctuations in the pulse profiles, so retrieval of a self-consistent pulse profile is harder. We would then expect the retrieved profile and retrieval error to change each time the simulation was re-run. To investigate the minimum required ensemble size, simulations (not shown as a figure) were run with ensemble sizes between 1 and 24 pulses. They demonstrated that there were significant variations in the retrieval error when the number of pulses was in the range 1-15, but that with larger ensemble sizes the retrieval error had only small fluctuations. We therefore suggest using at least 15 pulses to reduce the probability that outliers in the distributions strongly influence the measurements.

IV. EXPERIMENTAL WORK

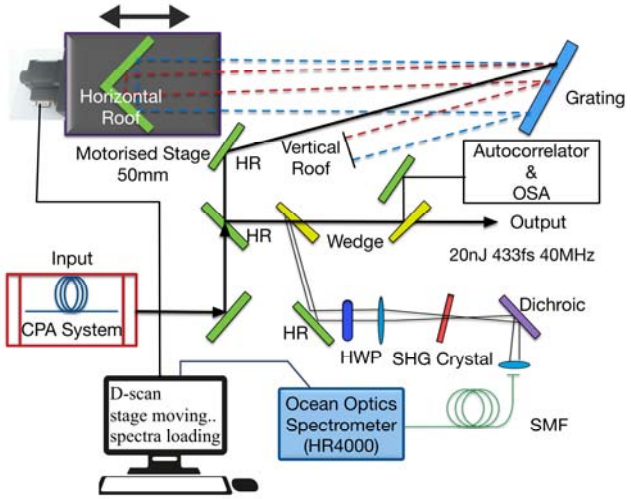

Fig. 9. Schematic of the experimental d-scan setup. See Ref. [21] for the CPA system amplifier configurations and performance details.

Our experimental testbed was developed in house and based closely on the Yb fiber CPA with a bendable final amplifier-fiber reported in [21]. In brief, we used a femtosecond Yb-doped fiber laser oscillator based on nonlinear polarization rotation, followed by an EOM pulse picker (not active here), a grating-based pulse stretcher, core-pumped pre-amplifiers, a large-mode-area cladding-pumped power amplifier and a standard Treacy compressor. The system was operated at the 40 MHz repetition rate of the seed oscillator to avoid nonlinear effects. The pulse energy was 20 nJ and the operating power was 0.8 W. The compressor setup and diagnostics for the d-scan are shown schematically in Fig. 9. A PC based Matlab algorithm recorded the fundamental spectrum output from the compressor (restricted-bandwidth), controlled the motorized stage under the horizontal-roof to perform the d- scan, recorded the SHG spectra, and operated the retrieval algorithm.

The compressor had a horizontal roof mirror to generate two passes of a single large grating and avoiding the need for a pair of gratings requiring independent alignment. The spectral phase offset applied by the compressor was:

$$\varphi(\omega) = \tilde{\varphi}(\omega) + \Delta L[\beta_2(\omega-\omega_0)^2/2 + (\omega-\omega_0)^3/6 + \beta_4(\omega-\omega_0)^4/24 + \beta_5(\omega-\omega_0)^5/120]. \quad (6)$$

Here, ΔL is the change in compressor grating separation when the horizontal roof-mirror is moved away from the minimum pulse-width position, and β_2, β_3, β_4, and β_5, are the second, third, fourth and fifth order dispersion coefficients: –0.0937 ps^2/mm, 0.001100 ps^3/mm, –2.1046 × 10^{-5} ps^4/mm, and 5.7001 × 10^{-7} ps^5/mm, respectively, at the central wavelength of 1045.0 nm. ($\tilde{\varphi}(\omega)$ accounts for the carrier-envelope offset and the time of transit of the pulse through the compressor, neither of which change the shape of the pulse envelope in the time domain.) The dispersion parameters were calculated to be accurate to within <0.2%, in view of the grating alignment tolerance of ~1 mrad and accurate measurement of the groove density on the grating. By far the dominant term is β_2, so in the algorithm we used β_2 = –0.0937 ps^2/mm to represent the applied GDD. The 50 mm travel motorized stage under the horizontal roof mirror adjusted the applied GDD range of ±2.350 ps^2 and 0.1 mm steps (0.094 ps^2) required 500 data points (i.e. SHG spectra). The acceleration and deceleration were set to low values and the data-acquisition was briefly delayed following each motion before recording the spectra to avoid vibrations. It takes a few seconds to move the grating and acquire an SHG spectrum. Typically, the total acquisition time was a few minutes. As noted in the Theory section, although the fine resolution increases the d-scan acquisition time it has benefits in terms of the retrieval process.

The diagnostics comprised an OSA (AQ6370, Yokogawa) for the fundamental spectrum, lens (f=10 cm) and SHG crystal (Type II BBO 10 mm × 10 mm × 0.5 mm), a dichroic mirror to separate out the residual fundamental and a spectrometer (HR4000, Ocean Optics) to record the SHG spectra. In the time-domain, a non-collinear SHG autocorrelator was used to verify the accuracy of the results obtained.

The results in Fig. 10 are shown with frequency offsets relative to the pulse central wavelength. In the d-scan map of Fig. 10(a), the dot-dash line shows G_o" (ω), i.e. the positions on the grid where the SHG maxima were recorded. (The GDD scan range (y-axis) is -2.0 ps^2 to +2.7 ps^2 because the motor travel was not in the center of the movement range at the position generating the shortest pulse.) The measured fundamental spectrum is shown in red in Fig. 10(d). The rapid convergence within five iterations of the algorithm is demonstrated by the plot of both the retrieved local error Err_G and global error Err_m in Fig. 10(b). The retrieved temporal pulse profile in Fig. 10(c) shows a small pre-pulse approximately 1 ps before the main pulse. The retrieved phase shown in blue in Fig. 10(d) is flat across the central part of the pulse spectrum but has a distortion on the high-frequency side.

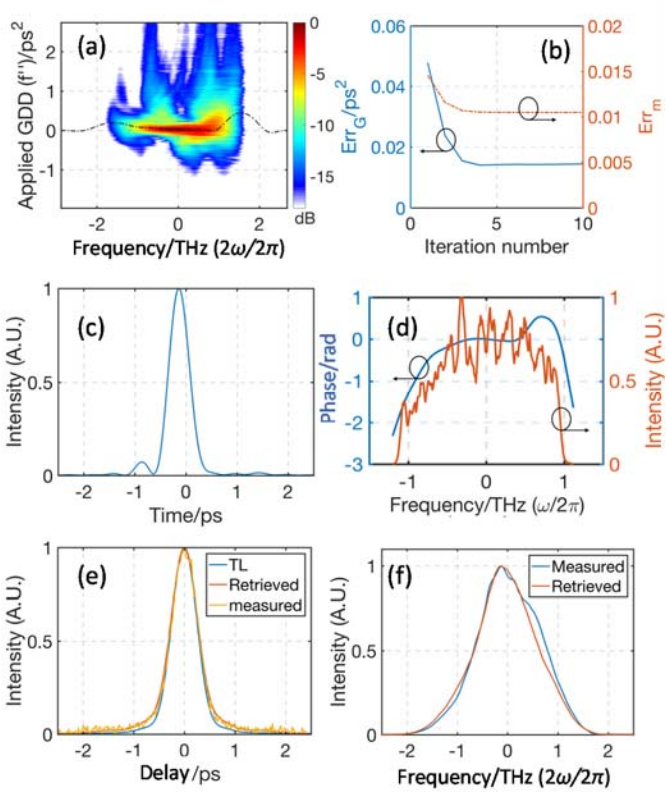

Fig. 10. (Color online.) Experimental d-scan phase retrieval results. Frequency offsets shown are relative to the pulse central wavelength of 1045 nm. (a) Colormap showing SHG spectra as a function of the applied GDD (d-scan); (b) retrieved GDD error, Err_G, and global error, Err_m, (c) calculated temporal pulse profile (d) retrieved phase and independently measured fundamental spectrum (e) measured autocorrelation trace compared with both the phase-distorted and transform limited calculated autocorrelation traces (f) measured and retrieved (calculated) SHG spectrum with the horizontal-roof mirror at the position that corresponds to the shortest measured SHG autocorrelation.

To verify the accuracy of the result, we used the retrieved phase with zero applied GDD to calculate the compressed pulse SHG autocorrelation. The calculated and measured data shown in Fig. 10(e) are in good agreement. (The transform limited pulse (blue curve) is shown for reference.) The pulse is ~ 1.1 times the transform-limited duration of 430 fs (rms). The corresponding measured and calculated SHG spectra are shown in Fig. 10(f).

TABLE II
SUMMARY OF SIMULATION RESULTS FOR SECTION 3.

Simulated pulse	τ_{TL_RMS} (fs)	τ_{RMS} (fs)	Δf_{FWHM} (THz)	τ_{RMS} / τ_{TL_RMS}	Applied phase profile	Err_G (ps^2)	$\mathbf{Err_\varphi}$	Fig. no.
Gaussian[a]	133	960	1.37	7.2	β_3 = 0.1 ps^3	0.98 x 10^{-3}	0.0282	NA
					β_4 =0.03 ps^4	4.6 x 10^{-3}	0.0575	
					β_5 =0.013 ps^5	4.1 x 10^{-3}	0.0569	
					Random phase	9.7 x 10^{-3}	0.0429	
Right-triangle[b]	204	1600	1.37	7.8	β_3 = 0.1 ps^3	0.3 x 10^{-3}	0.0032	3
					β_4 =0.03 ps^4	1.2 x 10^{-3}	0.0082	
					β_5 =0.013 ps^5	1.7 x 10^{-3}	0.0173	
					Random phase	3.0 x 10^{-3}	0.0291	
Gaussian[a] with SPM applied[c]	133	380	1.37	2.9	peak nonlinear phase = 3 radians	6.5 x 10^{-3}	0.0391	4(a, b)
Gaussian[a]: Step change in phase profile	133	1200	1.37	9.0	Phase: -0.3 ~ +0.3 THz 0 < -0.3 or > 0.3 THz -π	61.5 x 10^{-3}	1.18	5(a, b)
Gaussian[a]: slowly varying sinusoidal phase profile	133	364	1.37	2.7	Period=3 THz Amplitude=±π /2	4.06 x 10^{-3}	0.039	5(c, d)
Gaussian[a]: rapidly varying sinusoidal phase profile	133	2200	1.37	16.5	Period = 0.5 THz Amplitude=±π /2	0.31	1.32	5(e, f)
Double pulse: delayed replica [d]	133	969	1.37	7.3	Flat phase	NA	NA	6
Double pulse: Offset spectra, and different phase profiles [e]	83	216	3.15	2.6	Second pulse: offset 2 THz Dispersion applied: < 1 THz=0 > 1 THz = β_4=0.03 ps^4 centered at +2 THz	3.74 x 10^{-3}	0.097	7
Right-triangle[b] with pulse-to-pulse fluctuations[f]	204	1600	1.37	7.8	Random phase	5.59 x 10^{-3}	0.068	8

[a] corresponds to Gaussian pulses having a Gaussian spectral power density with bandwidth of 5 nm centered at 1045 nm.
[b] corresponds to right-triangle shaped spectrum with a bandwidth of 5 nm and centered at 1045 nm.
[c] when the pulse is strongly chirped (applied GDD is 100 ps^2)
[d] with relative pulse energies of E_2=4% of E_1: temporal offset of 5 ps.
[e] with relative energy of E_2=4% of E_1: second pulse has different spectral phase from that of the main pulse.
[f] only list the result of bandwidth fluctuations of 15%, other results are shown in fig. 8.

V. DISCUSSION AND SUMMARY

Phase retrieval and noise characterization of ultrashort pulse lasers is an important area of study that has led to several widely-used techniques. However, the cost and complexity of existing methods is typically only justified in research laboratories. The next generation of machining and ultrafast nonlinear imaging users require less complex and hence cheaper options. We report a method that quickly and inexpensively measures the phase of the pulses from fiber-based laser systems, which typically have narrower bandwidth and higher pulse-to-pulse fluctuations compared to Ti:sapphire lasers. It retains the intuitive interpretation and the ability to measure the average phase profile when pulse-to-pulse fluctuations are present which are demonstrated benefits of MIIPS. By using the fundamental laser spectrum to provide a self-consistency constraint an iterative algorithm calculates the spectral phase without requiring an SLM based pulse shaper. The technique has been shown to work reliably in the majority of cases except where the phase contained abrupt changes. Robust phase retrieval in the presence of laser fluctuations was confirmed using simulations on ensemble-averaged data and experimentally.

The experimental validation used data from an Yb-fiber CPA system with a motorized translation stage on the existing compressor grating setup to provide a dispersion scan through the position corresponding to the shortest output pulse. The retrieved phase results were in good agreement with the independently measured SHG autocorrelation. Although we treated an Yb-fiber CPA system in our simulations and experimental work, our approach can also be used with other lasers e.g., Er, Ho, and Tm fiber systems and Yb-solid state fs lasers. We suggest that this is a valuable addition to the range of characterization methods available.

ACKNOWLEDGMENT

We thank Mint Kunkel and Prof. James Leger, both at the University of Minnesota, for their valuable comments on the manuscript during preparation.

REFERENCES

[1] J. W. Nicholson, J. Jasapara, W. Rudolph, F. G. Omenetto, and A. J. Taylor, "Full-field characterization of femtosecond pulses by spectrum and cross-correlation measurements," *Optics Letters,* vol. 24, no. 23, pp. 1774-1776, 1999.

[2] R. Trebino *et al.*, "Measuring ultrashort laser pulses in the time-frequency domain using frequency-resolved optical gating," *Review of Scientific Instruments,* vol. 68, no. 9, pp. 3277-3295, Sep 1997.

[3] R. Trebino, *Frequency-Resolved Optical Gating: The Measurement of Ultrashort Laser Pulses*. Boston: Kluwer Academic, 2002.

[4] P. O'Shea, M. Kimmel, X. Gu, and R. Trebino, "Highly simplified device for ultrashort-pulse measurement," *Optics Letters,* vol. 26, no. 12, pp. 932-934, 2001.

[5] C. Iaconis and I. A. Walmsley, "Spectral phase interferometry for direct electric-field reconstruction of ultrashort optical pulses," *Optics Letters,* vol. 23, no. 10, pp. 792-794, 1998.

[6] V. V. Lozovoy, I. Pastirk, and M. Dantus, "Multiphoton intrapulse interference. IV. Ultrashort laser pulse spectral phase characterization and compensation," *Optics Letters,* vol. 29, no. 7, pp. 775-777, 2004.

[7] Y. Coello *et al.*, "Interference without an interferometer: a different approach to measuring, compressing, and shaping ultrashort laser pulses," *Journal of the Optical Society of America B,* vol. 25, no. 6, pp. A140-A150, 2008.

[8] M. Miranda *et al.*, "Characterization of broadband few-cycle laser pulses with the d-scan technique," *Optics Express,* vol. 20, no. 17, pp. 18732-18743, 2012.

[9] A. Comin, R. Ciesielski, N. Coca-López, and A. Hartschuh, "Phase retrieval of ultrashort laser pulses using a MIIPS algorithm," *Optics Express,* vol. 24, no. 3, pp. 2505-2512, 2016.

[10] M. Miranda, T. Fordell, C. Arnold, A. L'Huillier, and H. Crespo, "Simultaneous compression and characterization of ultrashort laser pulses using chirped mirrors and glass wedges," *Optics Express,* vol. 20, no. 1, pp. 688-697, 2012.

[11] F. Silva, M. Miranda, B. Alonso, J. Rauschenberger, V. Pervak, and H. Crespo, "Simultaneous compression, characterization and phase stabilization of GW-level 1.4 cycle VIS-NIR femtosecond pulses using a single dispersion-scan setup," *Optics Express,* vol. 22, no. 9, pp. 10181-10191, 2014.

[12] M. Miranda *et al.*, "Fast iterative retrieval algorithm for ultrashort pulse characterization using dispersion scans," *Journal of the Optical Society of America B,* vol. 34, no. 1, pp. 190-197, 2017.

[13] V. Loriot, G. Gitzinger, and N. Forget, "Self-referenced characterization of femtosecond laser pulses by chirp scan," *Optics Express,* vol. 21, no. 21, pp. 24879-24893, 2013.

[14] B. Xu, J. M. Gunn, J. M. D. Cruz, V. V. Lozovoy, and M. Dantus, "Quantitative investigation of the multiphoton intrapulse interference phase scan method for simultaneous phase measurement and compensation of femtosecond laser pulses," (in English), *Journal of the Optical Society of America B,* vol. 23, no. 4, pp. 750-759, 2006.

[15] V. V. Lozovoy, G. Rasskazov, D. Pestov, and M. Dantus, "Quantifying noise in ultrafast laser sources and its effect on nonlinear applications," *Optics Express,* vol. 23, no. 9, pp. 12037-12044, 2015.

[16] G. Rasskazov, V. V. Lozovoy, and M. Dantus, "Spectral amplitude and phase noise characterization of titanium-sapphire lasers," *Optics Express,* vol. 23, no. 18, pp. 23597-23602, 2015.

[17] Mathworks. (2017). *Smooth function in Matlab*. Available: https://uk.mathworks.com/help/curvefit/smooth.html

[18] D. N. Schimpf, E. Seise, J. Limpert, and A. Tünnermann, "The impact of spectral modulations on the contrast of pulses of nonlinear chirped-pulse amplification systems," *Optics Express,* vol. 16, no. 14, pp. 10664-10674, 2008.

[19] A. Comin, M. Rhodes, R. Ciesielski, R. Trebino, and A. Hartschuh, "Pulse characterization in ultrafast microscopy: A comparison of FROG, MIIPS and G-MIIPS," in *Conference on Lasers and Electro-Optics (CLEO) SW1H.5*, 2015.

[20] A. Comin, R. Ciesielski, G. Piredda, K. Donkers, and A. Hartschuh, "Compression of ultrashort laser pulses via gated multiphoton intrapulse interference phase scans," *Journal of the Optical Society of America B,* vol. 31, no. 5, pp. 1118-1125, 2014.

[21] J. S. Feehan, J. H. V. Price, T. J. Butcher, W. S. Brocklesby, J. G. Frey, and D. J. Richardson, "Efficient high-harmonic generation from a stable and compact ultrafast Yb-fiber laser producing 100 μJ, 350 fs pulses based on bendable photonic crystal fiber," *Applied Physics B,* vol. 123, no. 1, p. 43, 2017.

Yujun Feng received the B.Eng. (2012) and the Ph.D. (2017) degree in engineering physics from Tsinghua University, Beijing, China. In 2015, he joined High Power Fiber Laser (HPFL) group at the Optoelectronics Research Centre (ORC), University of Southampton, as a visiting Ph.D. student and is now a research fellow in this group. His research interests focus on high power and ultrafast fiber laser systems.

Johan Nilsson is a Professor at the ORC, University of Southampton, UK, and head of the High Power Fiber Lasers research group. In 1994, he received a doctorate in Engineering Science from the Royal Institute of Technology, Stockholm, Sweden, for research on optical amplification. Since then, he has worked on optical amplifiers and amplification in lightwave systems, optical communications, and guided-wave lasers, first at Samsung Electronics and later at ORC. His research has covered system, fabrication, and materials aspects, and in particular device aspects of high power fiber lasers and erbium-doped fiber amplifiers. He has published over 400 scientific articles. He is a fellow of the OSA and the SPIE, and a consultant to, and co-founder of, SPI Lasers. He is a member of the advisory board of the Journal of the Optical Society of Korea and was guest editor of two issues on high-power fiber lasers in IEEE Journal of Selected Topics in Quantum Electronics in 2009. He is a former chair of the Laser Science and Engineering technical group in OSAs Science and Engineering Council and is currently program chair for the EuroPhoton and Advanced Solid State Lasers conferences.

Jonathan H. V. Price received the Ph.D. degree in optoelectronics from the ORC, University of Southampton, U.K., in 2003. He then held a Royal Academy of Engineering Postdoctoral Research Fellowship at the ORC and has continued working in his main research areas of applied nonlinear fiber optics using novel glass types as well as silica microstructured optical fibers for ultrashort-pulse wavelength conversion applications / supercontinuum generation and the development of high-power femtosecond pulsed fiber laser sources.